Rapid Communications

Ab initio study of time-dependent dynamics in strong-field triple ionization

Jan H. Thiede and Bruno Eckhardt
Fachbereich Physik, Philipps-Universität Marburg, 35032 Marburg, Germany

Dmitry K. Efimov, Jakub S. Prauzner-Bechcicki, and Jakub Zakrzewski*
Instytut Fizyki im. Mariana Smoluchowskiego, Uniwersytet Jagielloński, Łojasiewicza 11, 30-348 Kraków, Poland

(Received 20 April 2018; revised manuscript received 10 July 2018; published 7 September 2018)

An *ab initio* analysis of strong-field three-electron ionization in a restricted-dimensionality model reveals the dynamics of the ionization process and the dominant channels for double (DI) and triple ionization (TI). Simulations using wave functions that respect the Pauli principle show that the most likely channel is a sequence of single ionization (SI) and DI, while direct TI has a much lower probability. The dominant DI process has the highest probability for a singlet of up- and down-spin electrons. The results demonstrate the significance of the Pauli principle for the selection of dominant pathways in ionization and possibly other many-electron processes in strong fields.

DOI: 10.1103/PhysRevA.98.031401

Ultrashort attosecond pulses enable studies of the fundamental aspects of the interaction between radiation and matter [1–3]. The generation of very high-order harmonics in the process is a key to the shaping of pulses and the realization of table-top sources of high-frequency coherent radiation [4] that may compete with complex synchrotron or free-electron laser sources [5]. High-intensity pulses can also result in multiple ionization, typically assisted by strong interactions between the escaping electrons [6–8]. Recently, the combination of both aspects, higher-order harmonic generation and multielectron effects, has moved into focus [9]. While there is an obvious need to study the strong-field multielectron processes, a full *ab initio* computation remains limited to the case of two-electron atoms (helium) at high frequencies, as studied by Taylor's group [10–13] (see also Refs. [14,15]), despite the huge progress in theory and computer power.

In the absence of full simulations, approximate methods become important, and semiclassical approaches [16–21] as well as simulations in a variety of models have been explored. For double ionization (DI), the Rochester model, in which the motion of each electron is restricted to the dimension set by the (linear) polarization of the laser field [22], has been studied. The model was applied to illustrate, e.g., the mechanism of the simultaneous ejection of two electrons at moderate intensity, and the transition to a sequential process for stronger fields (see, e.g., Refs. [23–25]). Despite its popularity, the model has its drawbacks: Electrons moving in parallel directions repel each other and this results in two-electron momentum distributions that disagree with observations. An adiabatic analysis allows one to locate the saddles in the potential for the electrons in the presence of an electric field, and such saddles act as transition states to efficient channels for ionization [26]. That analysis led to the development of an improved model in which electrons move along lines that pass through the saddles and are oblique to each other. The model takes electron correlations into account and gives a plausible representation of the ionization process [27,28]. A similar three-dimensional model is obtained by restricting the center-of-mass motion to the polarization axis; it captures similar aspects as the saddle picture (e.g., reproducing correctly the momenta distributions) [29–31], though with a larger number of degrees of freedom and at higher computational costs [32].

For the case of triple ionization (TI) studied here, several experimental results are available, especially for noble gases such as Kr, Ne, or Xe [33–38], but detailed theoretical studies are scarce, because of the even larger number of degrees of freedom. Some isolated aspects have been described in *classical* studies [39–43], often within restricted-dimensionality Rochester models. A notable quantum-mechanical effort [29,44] considered the TI of Li at high frequencies corresponding to synchrotron radiation, also within the Rochester model. Important progress has been made using different versions of multiconfiguration Hartree-Fock time-dependent orbitals [45] (for a review, see Ref. [46]). This method, however, depends on the number and an appropriate choice of initial orbitals included. Importantly, while it has been tested against quantum-mechanical results for the two-electron Rochester model, no such tests have been performed, as far as we are aware, for three-electron models since full quantum-mechanical analyses of the problem are still lacking.

The purpose of this Rapid Communication is to fill this gap, i.e., to provide a full *ab initio* quantum-mechanical analysis of TI for typical optical frequencies within the reduced dimensionality scheme. For the Hamiltonian, we consider models motivated by the adiabatic analysis of the classical dynamics [39], similar to that described above for DI. As the electric field changes slowly compared to electron dynamics we consider the possible ionization channels as realized close to the saddles of the instantaneous field value. The energetically lowest saddle corresponds to one with three electrons at the vertices of an equilateral triangle, in a plane perpendicular

*jakub.zakrzewski@uj.edu.pl

 ©2018 American Physical Society

to the field polarization axis [39]. When the field amplitude is varied the saddles move along straight lines that point radially outwards from the core: In the restricted model, the motion of the electrons is confined to these lines. As we will show, the analysis of the different sequential and simultaneous electron ejection processes provides a good understanding and explanation of the ionization yields.

The resulting Hamiltonian acting in an effective three-dimensional (3D) space takes the form (in atomic units)

$$H = \sum_{i=1}^{3} \frac{p_i^2}{2} + V(r_1, r_2, r_3), \tag{1}$$

with

$$V(r_1, r_2, r_3) = -\sum_{i=1}^{3} \left(\frac{3}{\sqrt{r_i^2 + \epsilon}} + \sqrt{\frac{2}{3}} F(t) r_i \right) + \sum_{i<j} \frac{1}{\sqrt{(r_i - r_j)^2 + r_i r_j + \epsilon}}, \tag{2}$$

where a parameter ϵ is responsible for smoothing of Coulomb singularity and, most importantly, allows us to match the ionization potential of our model with those of the real atom under study. We consider the case of Ne for which several experimental studies are available (although for longer pulses) [33,35–38]. More precisely, we consider a three-active-electron model of Ne, and the remaining electrons are assumed to be spectators. The ground-state energy of Ne is -4.63 a.u. [47], well approximated by the ground-state energy of $E_0 = -4.619$ a.u. for $\epsilon = 0.83$.

The time-dependent Schrödinger equation (TDSE) is solved on a spatial, equally spaced grid in three dimensions with Hamiltonian (1) by a standard fast Fourier transform (FFT) (split-operator) technique in an efficiently parallelized way [48]. The method is a straightforward generalization of our previous two-electron code [28] to three dimensions. However, accounting for the Pauli principle for three electrons is more subtle than for two electrons. While for two electrons one may restrict the evolution to spaces that are symmetric or antisymmetric under reflection of the position space wave functions [49], this is not the case for three electrons. Writing a properly symmetrized wave function for three electrons as a product of spatial and spin parts in not possible. The correct three-electron wave function has to be constructed as a Slater determinant, which, as shown in Ref. [44], reduces to

$$\Psi_{\alpha\alpha\beta}(r_1, r_2, r_3, t) \propto \alpha(1)\alpha(2)\beta(3)\psi_{12}(r_1, r_2, r_3, t) + \beta(1)\alpha(2)\alpha(3)\psi_{23}(r_1, r_2, r_3, t) + \alpha(1)\beta(2)\alpha(3)\psi_{13}(r_1, r_2, r_3, t), \tag{3}$$

where the single-electron spin functions correspond to $\alpha(i) \equiv |\uparrow\rangle_i$ and $\beta(i) \equiv |\downarrow\rangle_i$. To have a completely antisymmetric wave function, $\psi_{ij}(r_1, r_2, r_3, t)$ is antisymmetric under an exchange of i and j. As pointed out in Ref. [29], all three components of Ψ in the sum in Eq. (3) are orthogonal in spin space. Since the Hamiltonian (1) is spin independent, all three terms in the sum evolve independently, so that it is enough to evolve a single one and to obtain the remaining two by an appropriate change of indices. Assuming the wave function to be antisymmetric in r_1 and r_2 we find the appropriate ground state in this symmetry class by an imaginary time propagation of the TDSE, and this gives the ground-state energy $E = -4.619$ a.u. quoted above.

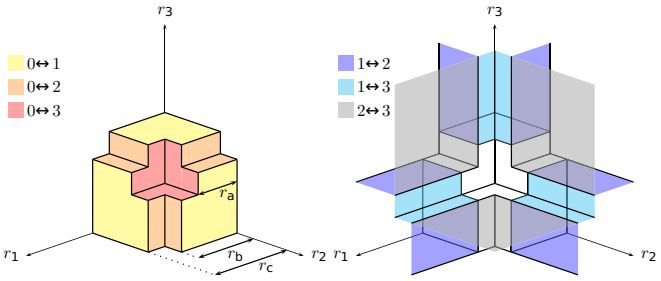

FIG. 1. Division of the position space for the calculation of the ion yields (only the first octant is shown). Region 0 (neutral atom) is the volume bounded by the yellow, orange, and red planes. Region 1 (singly ionized atom) is the union of the six volumes bounded by the yellow, cyan, and blue planes. Region 2 (doubly ionized atom) is the union of the 12 volumes bounded by the orange, blue, and gray planes. Region 3 (triply ionized atom) is the union of the eight volumes bounded by the red, cyan, and gray planes. The missing boundary planes of regions 1–3 are given by the absorbing boundary (not shown).

We here consider ionization by an extremely short, two-cycle pulse. While such short pulses are at the extreme limits of experimental availability, considerable progress towards their realization has been made [2,3,19,20,50,51]. The ionization process is then determined by few instances of time when the amplitude is large—that simplifies the detailed analysis of spin-dependent dynamics. For such a short pulse it is imperative to construct the envelope in such a way that the vector potential A vanishes after the pulse has passed [52]. We therefore take $F(t) = -\partial A/\partial t$ with

$$A(t) = -\frac{F_0}{\omega_0} \sin^2\left(\frac{\pi t}{T_p}\right) \sin(\omega_0 t + \varphi) \tag{4}$$

for $0 < t < T_p$, where φ defines the phase of the field under the pulse, n_c the number of cycles, and $T_p = 2\pi n_c/\omega_0$ the pulse duration. For the frequency, we take $\omega_0 = 0.06$, corresponding to a wavelength of 759 nm.

For the determination of the yields, we split the configuration space into different sectors and compute the fluxes across the boundaries, in an extension of the procedures used in Refs. [10,28,44]. The regions for the different states are composed of rectangular domains that are aligned with the coordinate axes, so that the boundaries between different regions consist of surfaces parallel to coordinate surfaces (compare Fig. 1). There is one region close to the nucleus, where all electrons are bound. There are three regions extended along the coordinate axes where one of the electrons is ionized and two are bound, another three regions where two electrons are free and one is bound, and finally a region far from the nucleus where all three electrons are free. For the distances defining the boundaries between the regions, we follow the idea of Ref. [10] and take different defining distances that allow one to distinguish between simultaneous and stepwise DI and TI. We take $r_c = 12.5$ a.u. for SI, $r_b = 7$ a.u. for DI, and

$r_a = 5$ a.u. for TI (Fig. 1). For instance, the region corresponding to a single charged ion has only one of the coordinates r_i large ($r_i > r_c$). Similarly, we can identify regions corresponding to DI and TI as described in the caption of Fig. 1.

The yields are determined by integrating the fluxes between the regions. The fluxes are determined by integrating the probability currents, which are given by

$$\mathbf{j}(\mathbf{r}, t) = \mathrm{Im}\,[\psi^*(\mathbf{r}, t)\nabla\psi(\mathbf{r}, t)] \tag{5}$$

in the length gauge or by

$$\mathbf{j}(\mathbf{r}, t) = \mathrm{Im}\,[\psi^*(\mathbf{r}, t)\nabla\psi(\mathbf{r}, t)] - \sqrt{2/3}|\psi(\mathbf{r}, t)|^2 A(t) \tag{6}$$

in the velocity gauge, with the vector potential $A(t)$. By Gauss's theorem, the fluxes determine the changes of the population in region $R \in \mathbb{R}^3$ according to

$$\begin{aligned}\frac{\partial}{\partial t} P_R(\mathbf{r}, t) &= \frac{\partial}{\partial t} \iiint_R |\psi(\mathbf{r}, t)|^2 d^3\mathbf{r} \\ &= -\iiint_R \nabla \cdot \mathbf{j}(\mathbf{r}, t) d^3\mathbf{r} \\ &= -\iint_{\partial R} \mathbf{j}(\mathbf{r}, t) \cdot d\sigma \equiv f_R(t),\end{aligned} \tag{7}$$

where ∂R is the border of region R and $d\sigma$ is the corresponding surface element. We assume that the wave function decreases sufficiently rapidly as $r \to \infty$ so that all the above integrals converge for any region R. Correspondingly, the instantaneous value of the population in region R is given by

$$P_R(\mathbf{r}, t) = P_R(\mathbf{r}, 0) - \int_0^t f_R(t')dt'. \tag{8}$$

We have checked that changes of the defining distances affect the ionization probabilities quantitatively only, leaving the qualitative picture, which is our aim with the reduced dimensionality model, unaffected. By considering which electron travels outside the bound-state region we can identify which spin channels are most vulnerable to ionization—recall that the antisymmetric configuration space wave function corresponds to a majority spin pointing up.

Let us first consider the yields obtained for a pulse (4) for different values of the field peak amplitude F_0, as shown in Fig. 2 and $\varphi = 0$. One observes a fast saturation of SI that reveals, upon close inspection of the data, a shallow maximum around $F_0 = 0.2$, followed by a decay for larger amplitudes when DI and then TI become important. From the contributions to the DI yield, we can determine the ratio of 0-1-2 (sequential DI) to 0-2 (NSDI). Similarly, for TI we may define sequences such as 0-2-3 or 0-1-3, corresponding to combinations of SI and DI in different orders, or 0-3, a simultaneous TI process. Note that the flux method does not allow us to distinguish a sequential 0-1-2-3 process from a nonsequential 0-2-3 scenario, since the integrated flux across the 2-3 border determines the 0-2-3 process which contains in the 0-2 part both the sequential 0-1-2 and a direct 0-2 path. However, we know the effectiveness of the 0-1-2 vs 0-2 channel from the corresponding fluxes, and assuming that the same ratio holds for three-electron processes, we may deduce approximate values for the corresponding yields in TI. The results for the yields and the different contributions for a two-cycle pulse are shown in Fig. 2.

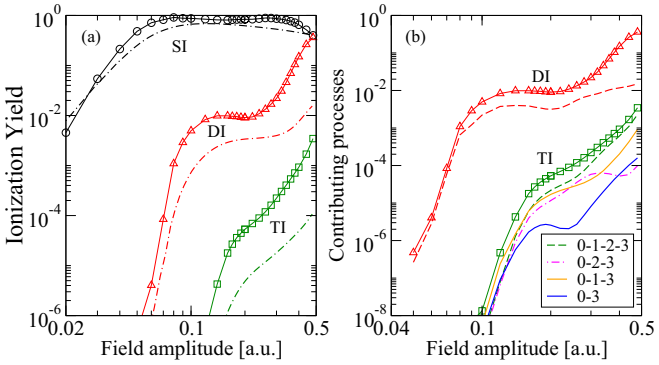

FIG. 2. Numerical ionization yields for a two-cycle pulse as a function of top electric field amplitude in atomic units. $F_0 = 0.1$ a.u. corresponds to 5.14×10^{10} V/m and laser intensity $I = 3.5 \times 10^{14}$ W/cm^2. Left panel: Total yields (probabilities) for single ionization (SI, black circles), double ionization (DI, red triangles), and triple ionization (TI, green squares). The continuous lines are from the model, and dashed-dotted lines after integration over a Gaussian beam (9). SI saturates over a wide range of field strengths and DI shows a pronounced knee structure, TI a weak one. Right panel: Different contributions to DI and TI, over a smaller range of field amplitudes. The red dashed lines show the nonsequential double-ionization (NSDI) contribution to DI, which is overtaken by sequential processes for higher intensities. The legend identifies four contributions to TI, with the sequential process being the dominant and direct TI the weakest contribution.

In the experiment, atoms are illuminated by a Gaussian laser beam. In the computations, this can be accounted for by averaging the yields over the laser beam intensity profile. As shown in Ref. [53], the averaged ionization yields $S(I_0)$ may simply be obtained as

$$S(I_0) \propto \int_0^{I_0} dI\, P(I)/I, \tag{9}$$

where $I_0 \propto F_0^2$ is the peak intensity at the focal point and $P(I)$ is a fraction obtained numerically for a given peak intensity I. The results of such an averaging are shown as dashed-dotted lines in the left panel of Fig. 2. Note that the knee structure, indicating the transition from the nonsequential processes to the sequential ones, becomes significantly smoothed out and the resulting average yields resemble qualitatively the ones observed in experiments for Ne [33,35–38].

The dominant feature in Fig. 2 is a deep knee structure for a DI, mostly due to NSDI (as indicated by the red curves). This happens in the same interval of field amplitudes as the saturation, together with a small drop of the single ionization yield. For stronger fields, the fraction of NSDI becomes less significant in the total DI yield, and we recover the sequential path familiar from earlier studies. For even stronger intensities, TI sets in with less pronounced saddles. Note that direct TI is the least probable scenario, with DI (either sequential or NSDI) followed by a SI process being the most effective process.

The access to the time-dependent fluxes across the different borders also provides information about the spin polarization of the outgoing electrons. Recall that our three-electron initial wave function is composed of two spin-up electrons (here

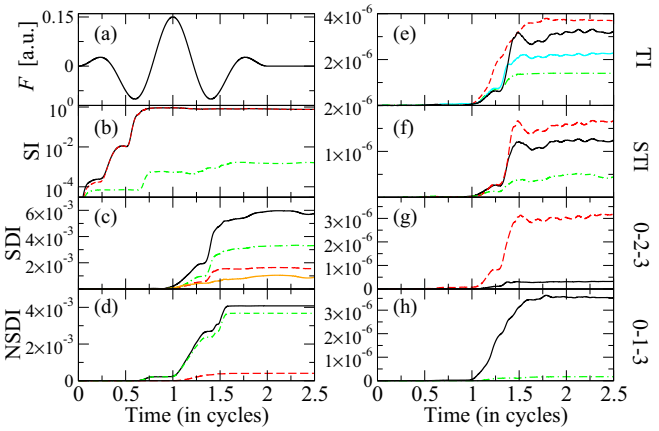

FIG. 3. Spin-resolved time dependence of different ionization processes for $F_0 = 0.15$ and $\varphi = 0$. The left column shows contributions to SI and DI, and the right column to TI. (a) shows the pulse shape. (b) SI (black line) is dominated by U electron emission (red dashed), while ionization of the D electron (green dashed) has a much smaller probability. (c) shows that sequential double ionization (SDI) (black line) is composed of the dominant 0-U-D channel (green dashed-dotted), with only small contributions from the 0-U-U channel (red dashed line) and minor contributions from the path 0-D-U (orange) in which the D electron is ejected first. For NSDI (d) shows that the product DU (green dashed-dotted) is strongly favored compared to UU emission (red-dashed) – with black line giving the total NSDI. In the right column, (e) shows contributions to TI: sequential TI (STI) 0-1-2-3 (cyan), 0-2-3 channel (black), 0-1-3 (red dashed line), and 0-3 (green dashed line). (f) resolves the spin contributions to STI, with black, red-dashed, and green dotted-dashed curves corresponding to U-U-D, U-D-U, and D-U-U sequential emissions. (g) resolves the 0-2-3 DI followed by a single emission channel, and shows that the DU-U path (red) is more prominent than the UU-D sequence (black); (h) for the 0-1-3 channel the first SI is predominantly via the U electron followed by the UD pair (black) while D-UU (green dashed) is negligible.

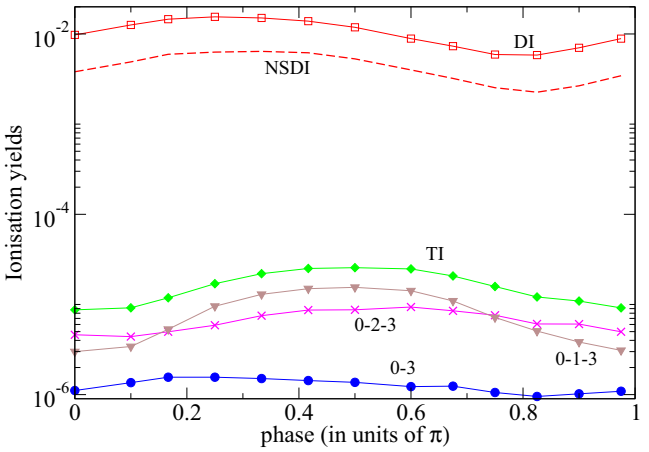

FIG. 4. The dependence of different ionization yields (indicated in the figure) on the carrier envelope phase φ in Eq. (4). The data correspond to $F_0 = 0.15$. Observe that the importance of different paths for triple ionization may depend on φ.

denote by U) and one spin-down electron (denoted by D). The wave function is antisymmetric with respect to the exchange of U electrons, and symmetric with respect to an exchange between U and D electrons. The fluxes allow us to address the question whether it is more probable to eject first a U or a D electron. Intuition suggests that if one of the U's and D form a singlet, the remaining U electron is easier to ionize. And, indeed, the SI yield for the D electron is negligible (compare Fig. 3). Since our approach gives us a direct access to time-dependent fluxes by defining appropriate ionization processes, we can in a similar way analyze DI and TI events. In particular, such an analysis points towards DU emission as a dominant channel for NSDI, with the simultaneous emission of two U electrons being much less probable. Similarly, we may identify the dominant channels for TI. After splitting the 0-2-3 channel into the sequential 0-1-2-3 and NSDI followed by single-electron emission, the leading channel becomes 0-1-3 for low-field amplitude. In such a case of SI followed by the simultaneous ejection of the remaining two electrons, the first stage is almost surely performed by the U electron. On the other hand, the often neglected 0-2-3 channel [33] may be the leading TI channel for intermediate-field values. All the possible channels are described in the caption of Fig. 3.

For the short two-cycle pulse used in calculations the shape and maximal amplitude (for a given F_0) depend on the carrier envelope phase (CEP) φ [see (4)]. The effects on the yields are shown in Fig. 4. One observes that CEP values for the most effective DI and TI are different. Moreover, the efficiency of different TI channels depends on CEP, e.g., the efficiency of 0-1-3 and 0-2-3 TI channels may be reversed (we here do not separate the 0-2-3 process further for simplicity). Regardless of the CEP value the direct 0-3 ionization channel is the least effective. On the other hand, the main feature, i.e., that U (majority population) electrons ionize first, does not depend on details of the pulse. Similarly, in nonsequential processes, it is a "singlet" pair UD which is more likely to be ejected than a UU combination.

The present Rapid Communication paves the way towards a detailed analysis of the dynamics of three-active-electron dynamics for Li as well as other noble gases and for longer pulses. While we have concentrated on the ionization yield and the dynamics of the process, work is in progress concerning the high-order harmonic generation and ion momenta distribution analysis.

The support of PL-Grid Infrastructure essential for obtaining the numerical results presented is acknowledged. We acknowledge support of the National Science Centre, Poland via Project No. 2016/20/W/ST4/00314 (D.E., J.P.B., and J.Z.). Support by EU FET-PRO QUIC is also acknowledged.

[1] F. Krausz and M. Ivanov, Rev. Mod. Phys. **81**, 163 (2009).

[2] F. Calegari, G. Sansone, S. Stagira, C. Vozzi, and M. Nisoli, J. Phys. B: At., Mol. Opt. Phys. **49**, 062001 (2016).

[3] M. F. Ciappina, J. Pérez-Hernández, A. Landsman, W. Okell, S. Zherebtsov, B. Förg, J. Schötz, L. Seiffert, T. Fennel, T. Shaaran *et al.*, Rep. Prog. Phys. **80**, 054401 (2017).

[4] T. Popmintchev, M.-C. Chen, P. Arpin, M. M. Murnane, and H. C. Kapteyn, Nat. Photonics **4**, 822 (2010).
[5] J. D. Bozek, Eur. Phys. J.: Spec. Top. **169**, 129 (2009).
[6] A. l'Huillier, L. A. Lompre, G. Mainfray, and C. Manus, Phys. Rev. A **27**, 2503 (1983).
[7] T. S. Luk, U. Johann, H. Egger, H. Pummer, and C. K. Rhodes, Phys. Rev. A **32**, 214 (1985).
[8] S. Larochelle, A. Talebpour, and S.-L. Chin, J. Phys. B: At., Mol. Opt. Phys. **31**, 1201 (1998).
[9] P. M. Abanador, F. Mauger, K. Lopata, M. B. Gaarde, and K. J. Schafer, Phys. Rev. A **97**, 043414 (2018).
[10] D. Dundas, K. T. Taylor, J. S. Parker, and E. S. Smyth, J. Phys. B: At., Mol. Opt. Phys. **32**, L231 (1999).
[11] K. T. Taylor, J. S. Parker, K. J. Meharg, and D. Dundas, Eur. Phys. J. D **26**, 67 (2003).
[12] J. S. Parker, L. R. Moore, D. Dundas, and K. T. Taylor, J. Phys. B: At., Mol. Opt. Phys. **33**, L691 (2000).
[13] A. Emmanouilidou, J. S. Parker, L. R. Moore, and K. T. Taylor, New J. Phys. **13**, 043001 (2011).
[14] J. Feist, S. Nagele, R. Pazourek, E. Persson, B. I. Schneider, L. A. Collins, and J. Burgdörfer, Phys. Rev. A **77**, 043420 (2008).
[15] R. Pazourek, J. Feist, S. Nagele, and J. Burgdörfer, Phys. Rev. Lett. **108**, 163001 (2012).
[16] K. J. Schafer, B. Yang, L. F. DiMauro, and K. C. Kulander, Phys. Rev. Lett. **70**, 1599 (1993).
[17] P. B. Corkum, Phys. Rev. Lett. **71**, 1994 (1993).
[18] M. Lewenstein, P. Balcou, M. Y. Ivanov, A. L'Huillier, and P. B. Corkum, Phys. Rev. A **49**, 2117 (1994).
[19] M. Kübel, C. Burger, N. G. Kling, T. Pischke, L. Beaufore, I. Ben-Itzhak, G. G. Paulus, J. Ullrich, T. Pfeifer, R. Moshammer, M. F. Kling, and B. Bergues, Phys. Rev. A **93**, 053422 (2016).
[20] A. Chen, M. Kübel, B. Bergues, M. F. Kling, and A. Emmanouilidou, Sci. Rep. **7**, 7488 (2017).
[21] D. B. Milošević, Phys. Rev. A **96**, 023413 (2017).
[22] R. Grobe and J. H. Eberly, Phys. Rev. Lett. **68**, 2905 (1992).
[23] D. Bauer, Phys. Rev. A **56**, 3028 (1997).
[24] W.-C. Liu, J. H. Eberly, S. L. Haan, and R. Grobe, Phys. Rev. Lett. **83**, 520 (1999).
[25] M. Lein, E. K. U. Gross, and V. Engel, Phys. Rev. Lett. **85**, 4707 (2000).
[26] B. Eckhardt and K. Sacha, J. Phys. B: At., Mol. Opt. Phys. **39**, 3865 (2006).
[27] J. S. Prauzner-Bechcicki, K. Sacha, B. Eckhardt, and J. Zakrzewski, Phys. Rev. Lett. **98**, 203002 (2007).
[28] J. S. Prauzner-Bechcicki, K. Sacha, B. Eckhardt, and J. Zakrzewski, Phys. Rev. A **78**, 013419 (2008).
[29] C. Ruiz, L. Plaja, and L. Roso, Laser Phys. **16**, 600 (2006).
[30] A. Staudte, C. Ruiz, M. Schöffler, S. Schössler, D. Zeidler, T. Weber, M. Meckel, D. M. Villeneuve, P. B. Corkum, A. Becker, and R. Dörner, Phys. Rev. Lett. **99**, 263002 (2007).
[31] S. Chen, C. Ruiz, and A. Becker, Phys. Rev. A **82**, 033426 (2010).
[32] D. K. Efimov, A. Maksymov, J. S. Prauzner-Bechcicki, J. Thiede, B. Eckhardt, A. Chacon, M. Lewenstein, and J. Zakrzewski, Phys. Rev. A **98**, 013405 (2018).
[33] B. Feuerstein, R. Moshammer, and J. Ullrich, J. Phys. B: At., Mol. Opt. Phys. **33**, L823 (2000).
[34] A. Rudenko, K. Zrost, B. Feuerstein, V. L. B. de Jesus, C. D. Schröter, R. Moshammer, and J. Ullrich, Phys. Rev. Lett. **93**, 253001 (2004).
[35] S. Palaniyappan, A. DiChiara, E. Chowdhury, A. Falkowski, G. Ongadi, E. L. Huskins, and B. C. Walker, Phys. Rev. Lett. **94**, 243003 (2005).
[36] K. Zrost, A. Rudenko, T. Ergler, B. Feuerstein, V. de Jesus, C. Schröter, R. Moshammer, and J. Ullrich, J. Phys. B: At., Mol. Opt. Phys. **39**, S371 (2006).
[37] A. Rudenko, T. Ergler, K. Zrost, B. Feuerstein, V. de Jesus, C. Schröter, R. Moshammer, and J. Ullrich, J. Phys. B: At., Mol. Opt. Phys. **41**, 081006 (2008).
[38] N. Ekanayake, S. Luo, B. L. Wen, L. E. Howard, S. J. Wells, M. Videtto, C. Mancuso, T. Stanev, Z. Condon, S. LeMar, A. D. Camilo, R. Toth, W. B. Crosby, P. D. Grugan, M. F. Decamp, and B. C. Walker, Phys. Rev. A **86**, 043402 (2012).
[39] K. Sacha and B. Eckhardt, Phys. Rev. A **64**, 053401 (2001).
[40] P. J. Ho and J. H. Eberly, Phys. Rev. Lett. **97**, 083001 (2006).
[41] P. J. Ho and J. H. Eberly, Opt. Express **15**, 1845 (2007).
[42] J. Guo and X.-s. Liu, Phys. Rev. A **78**, 013401 (2008).
[43] Y. Zhou, Q. Liao, and P. Lu, Opt. Express **18**, 16025 (2010).
[44] C. Ruiz, L. Plaja, and L. Roso, Phys. Rev. Lett. **94**, 063002 (2005).
[45] R. Anzaki, T. Sato, and K. L. Ishikawa, Phys. Chem. Chem. Phys **19**, 22008 (2017).
[46] K. L. Ishikawa and T. Sato, IEEE J. Sel. Top. Quantum Electron. **21**, 1 (2015).
[47] A. Kramida, Y. Ralchenko, and J. Reader, NIST Atomic Spectra Database Version 5.5.6, 2018, http://www.nist.gov/pml/atomic-spectra-database.
[48] J. H. Thiede, Multiple ionization in strong laser fields, Ph.D. thesis, Marburg University, 2017.
[49] B. Eckhardt, J. S. Prauzner-Bechcicki, K. Sacha, and J. Zakrzewski, Phys. Rev. A **77**, 015402 (2008).
[50] K. T. Kim, C. Zhang, T. Ruchon, J.-F. Hergott, T. Auguste, D. M. Villeneuve, P. B. Corkum, and F. Quéré, Nat. Photonics **7**, 651 (2013).
[51] M. Ossiander, F. Siegrist, V. Shirvanyan, R. Pazourek, A. Sommer, T. Latka, A. Guggenmos, S. Nagele, J. Feist, J. Burgdörfer, R. Kienberger, and M. Schultze, Nat. Phys. **13**, 280 (2016).
[52] B. Eckhardt, J. S. Prauzner-Bechcicki, K. Sacha, and J. Zakrzewski, Chem. Phys. **370**, 168 (2010).
[53] J. Strohaber, A. Kolomenskii, and H. Schuessler, J. Appl. Phys. **118**, 083107 (2015).